27th Symposium on Naval Hydrodynamics
Seoul, Korea, 5-10 October 2008

# Simulation of the Incompressible Viscous Flow around Ducted Propellers with Rudders Using a RANSE Solver

A. Sánchez-Caja,[1] J.V. Pylkkänen[2] and Tuomas P. Sipilä[1]
([1,2]VTT Technical Research Center of Finland, [2]ret.)

**ABSTRACT**

Within EU Project SUPERPROP, fishing vessels have been studied. Usually their propulsion units consist of ducted propellers in order to provide large thrust in trawling. Rudders may significantly influence the performance of ducted propellers especially if they are located at short distance from the duct. This paper summarizes some of the CFD calculations performed as the starting point for the development of a new propeller design for a reference fishing boat. The basic design performance particulars were obtained from the analysis of the existing conventional ducted propeller installed in the ship. The flow around the original propeller geometry and around one of the alternative designs is simulated using RANS code FINFLO. As a part of the project the rudder blockage effect has been investigated using a quasi-steady approach.

**INTRODUCTION**

Within EU Project SUPERPROP, fishing vessels have been studied to improve their operational costs. Generally, the operational profile of such vessels includes two distinct working conditions. In free running, they need a relatively high speed to reach the fisheries in a short time. In trawling, they operate at low speed with the nets filled with fish and with propellers heavily loaded. Ducted propellers are suitable for meeting the latter condition efficiently. Usually the design point is selected as a compromise between the two situations.

During the lifetime of the vessel propeller efficiency deteriorates as a consequence of roughness increase on both propeller and hull. If operational costs are to be kept low, the propeller efficiency should be optimized not only initially for the design operation point but also for the operational life of the propeller. Sometimes by re-machining the blades, the propeller can be accommodated to the new operating conditions with low costs. In other cases a new propeller design may be the cheapest solution.

A reference fishing boat with an old ducted propeller was selected as test case for hydrodynamic analysis in the SUPERPROP project. The existing ducted propeller installed in the ship was analyzed and was found to be over-pitched for the present situation after several years of operation. A new design point was established with the agreement of the ship owner and different alternatives were studied to adapt the existing propeller to the actual working point. They included blade cutting and re-pitching of the propeller. Blade cutting was discarded as solution due to the alteration of the strength properties of the blade. The design condition would be only reached by large cuts of the chord, which additionally would result in a strong reduction of the expanded blade area of the propeller and consequently, in significant cavitation problems. A new propeller design was considered a more appropriate solution. This paper presents the hydrodynamic numerical analysis for the existing ducted propeller and rudder of the reference vessel. Additionally, several propeller designs were made and the numerical analysis of an alternative ducted propeller design is presented.

The interaction between the propeller and rudder has been numerically investigated by several researchers. Moriyama (1981) developed an estimation method for the propeller-rudder interaction by applying thick wing theory and boundary layer theory to a rudder with thickness. His calculation results include the effects of rudder and propeller-rudder gap on the propeller performance coefficients. Suzuki, Toda, and Suzuki (1993) performed viscous flow computations of propeller-rudder interaction. The steady flow field was calculated by a viscous flow code coupled with a body force distribution which represented the propeller. He gives also the effect of the rudder on powering performance coefficients. Tamashima, Mori, Matsui, Yamazaki, and Yang (1993) use infinitely bladed

theory to simulate the propeller. A panel method was applied for the rudder. The friction forces on the rudder were obtained by two-dimensional boundary layer theory. Li (1995) developed a linear method to model propeller-rudder interaction. His sample calculation results include $\Delta K_T$ versus $J$ for different propeller-rudder gaps, $\Delta K_T$ versus $J$ for different thickness/chord values, and open water results with and without rudder behind. Coupled potential methods for the analysis of propeller-rudder interaction via circumferential averaged flow are also found in Lee et al. (2003), Greco and Salvatore (2004), Kinnas et al. (2007). Han (2008) studied hull/propeller/rudder interaction by coupling a RANS solver to either a vortex lattice lifting surface or a lifting line propeller model via body forces.

In this paper the RANS equations are solved for simulating the flow around a ducted propeller and rudder. The actual geometry for both ducted propeller and rudder is modeled without any simplification. In principle such computations may be made in three different ways: full unsteady (Sánchez-Caja et al, 1999), quasi-steady and steady-averaged (Sánchez-Caja et al, 2003). In the first case time effects are fully accounted for, but computational times are long for large meshes. In the second case the propeller block is rotating but fixed for the calculation at one angular position. Here, memory (time) effects are not included, but lack of flow symmetry is present to some degree on the propeller blades. In the third case the flow quantities are circumferentially averaged on an axisymmetric surface (mixing-plane) located midway between the propeller and the rudder, and memory effects are not included. The advantage of the two latter approaches is that they give an indication of the global performance for the propulsor unit within a reasonable computational time. The computations presented in this paper were made using a quasi-steady approach. Some tests not reported in this paper were made also following a steady-average approach.

## NUMERICAL METHODS

The flow simulation in FINFLO is based on the solution of the RANS equations by the pseudo-compressibility method. FINFLO solves the RANS equations by a finite volume method. The solution is extended to the wall and is based on approximately factorized time-integration with local time-stepping. The code uses either Roe's flux-difference splitting or Van Leer's flux-vector splitting for compressible flows and an upwind-based scheme for incompressible flows. In the latter case, the pressure is center-differenced and a damping term is added via a convective velocity. A multigrid method is used for the acceleration of convergence. Solutions in coarse grid levels are used as starting point for the calculation in order to accelerate convergence. A detailed description of the numerical method including discretization of the governing equations, solution algorithm, etc. can be found in Sanchez-Caja et al. (1999 and 2000). Chien's k-epsilon turbulence model was used in the calculation.

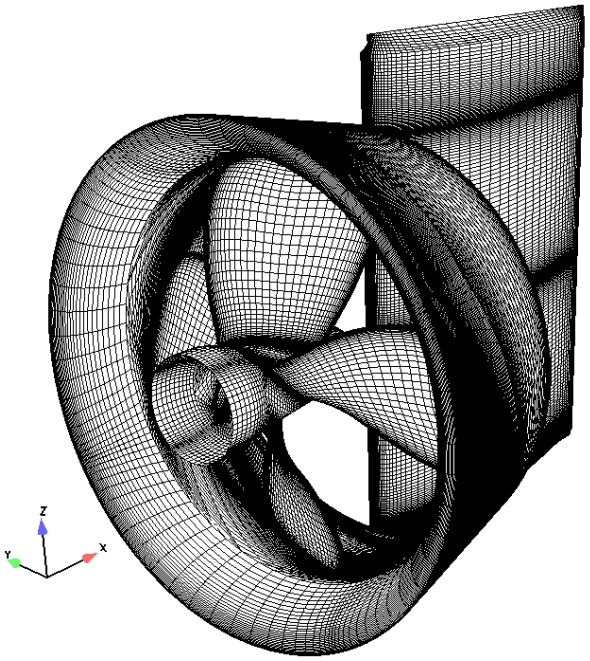


*Figure 1. Computational mesh on the propeller, duct and rudder surfaces. Original propeller*

There are two ways to approximate unsteady rotational flows. The first one is called a quasi-steady or multiple reference frame solution and the second one a mixing-plane approach. In both approaches the rotating and non-rotating blocks are firstly connected in an ordinary way. Since global Cartesian velocity components are used no coordinate transformation is necessary. In the mixing-plane approach the flow quantities for both the rotating and non-rotating blocks are circumferentially averaged on both sides of the common face and then transferred to the ghost cells as boundary values. The flux calculation on the boundary is done in an ordinary way. The procedure approximates a situation, where the boundary values oscillate at a high frequency making the averaging sensible.

In the quasi-steady approach the rotating and non-rotating blocks are connected without any averaging process. The solution approximates a situation, where the rotating block is frozen to a particular position. As rotating and non-rotating blocks are connected together, the flux calculation differs in those blocks. In

the rotating frame of reference, the rotational speed affects the convective speed that is relative to a cell surface. Furthermore in a rotating frame of reference there is a source term in the momentum equation. As a result the solution may exhibit special features, if the flow is not uniform (Sipilä, 2008). E.g. any flow disturbance from for example an upstream non-rotating block will seem to rotate when traveling through the downstream rotating one, or vice versa. In other words, although the absolute velocities will vary in a smooth continuous way through the interface, the flow disturbances (wakes) will propagate changing direction at the interface. This means that the angular location of a propeller blade in a quasi-steady computation will not correspond to the same location of the blade in a time-accurate computation. This clearly differs from the quasi-steady computations made in panel methods where such correspondence may be established. In the mixing-plane approach the averaging generates a homogeneous boundary condition; hence the interpretation of the solution from a physical standpoint is simpler than that resulting from a quasi-steady approach.

In order to keep the numerical interaction between the rotating and non-rotating domains weak the interface should be located far enough from solid surfaces (i.e. propeller blades and rudder), being more critical this remark for the downstream block.

## GEOMETRY AND MESH

The propeller geometry was obtained by direct measurements and transformed to IGES format. The propeller was a four-bladed one with 2.6 m diameter and about 0.96 pitch diameter ratio.

The computational mesh of the original propeller was generated with the IGG grid program and an in-house built program. The mesh was structured and continuous. The use of overlapping or non-matching blocks was avoided. C-topology was selected around the propeller blades, which allowed having cells concentrated on the propeller wake. O-topology was used around the duct and H around the rudder. Computational cells were concentrated in the duct wake and propeller hub vortex zone.

The grids used in the present calculations consisted of 9.5 million cells distributed in 23 blocks. The calculation was made at model scale. Figure 1 shows a view of the computational mesh on the propeller, duct and rudder surfaces. The proximity of the rudder to the nozzle made it difficult the construction of the structured mesh. The mesh of the alternative propeller design was similar to that of the original propeller, but Kaplan type blade shape was used instead. Figures 2 and 3 show from a fore and back view respectively details of the grid construction.

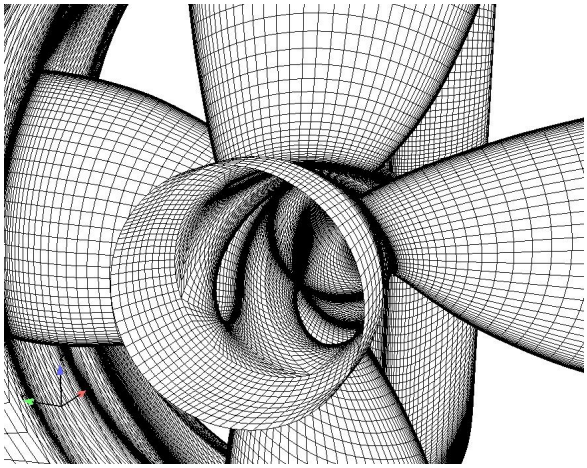

*Figure 2. Detail of grid construction on hub & blade. Fore view of propeller mesh for the alternative design.*

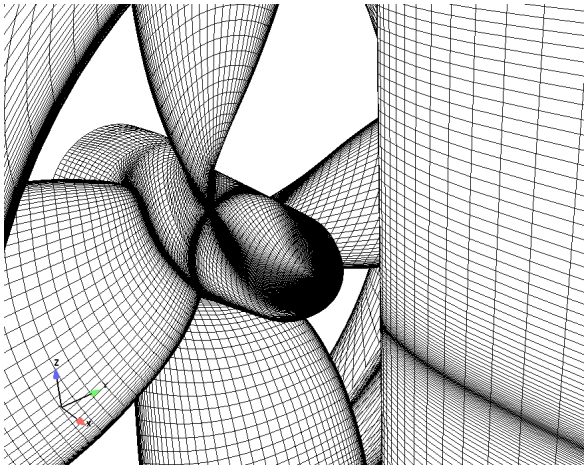

*Figure 3. Detail of grid construction on hub & rudder. Back view of propeller mesh for the alternative design.*

## BOUNDARY CONDITIONS

The boundary conditions were as follows. The downstream cap of the hub and surfaces of the propeller blades are rotating solid walls with boundary conditions enforcing the velocity field to match the propeller rotational speed. The duct and rudder surfaces are non-rotating solid walls. At the computational infinity the boundary conditions consist of uniform flow applied to the inlet and peripheral surfaces, and zero streamwise gradients of the flow variables as well as zero pressure difference at the

outlet. For the calculation without rudder the boundary conditions were as those in the calculation with rudder, but cyclic boundary conditions were applied to benefit from the periodicity of the flow.

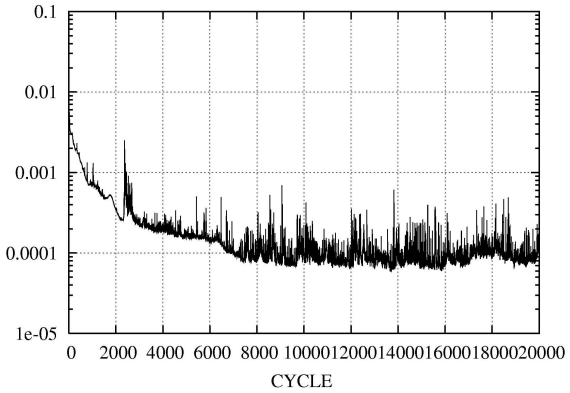


*Figure 4. Convergence history of residuals for x-momentum in the second grid level (medium grid).*

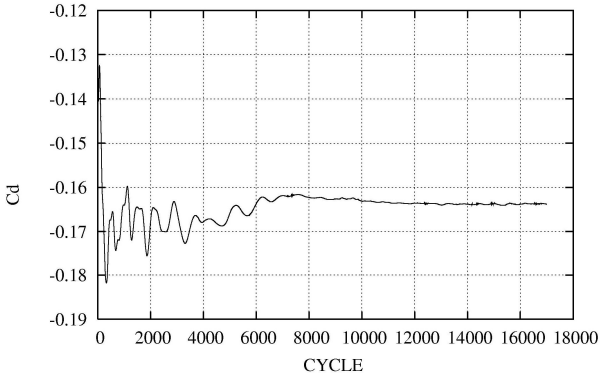


*Figure 5. Convergence history of an overall drag coefficient for the first grid level (fine grid).*

## CONVERGENCE AND ANALYSIS OF FORCES

Only one propeller position was analyzed in quasi-steady flow. Even though the forces on each individual blade may vary significantly as the propeller rotates, the total force over all the blades do not vary so much. This makes the computations representative of the average performance to a resolution degree of the total fluctuation amplitude.

The computations were performed on Xeon™ with 8 or 9 3.0 GHz processors. In solving the differential equations the multigrid method was applied with two multigrid levels for acceleration of convergence. In some critical zones the multigrid level was one. Convergence was also accelerated by starting the calculation with the solution on medium and coarse meshes corresponding to the 2nd and 3rd grid levels. The coarse grid levels are obtained by removing every other grid line in each direction from the mesh of the previous grid level. Figure 4 shows the convergence history of residuals for x-momentum in the 2nd grid level corresponding to the calculation of one of the ducted propellers with rudder. Figure 5 shows the convergence of drag for the 1st grid level.

Computations were made first for the ducted propeller without rudder in uniform flow at an advance number corresponding to the new design condition. The solution is time-independent. The advance number was estimated from an average effective wake for the entire ducted propeller unit obtained with the help of an actuator disk model coupled with RANS solver FINFLO (Sánchez-Caja et al. 2007). Model test measurements were available for the ducted propeller without rudder in open water. Table I compares computational results to measurements. The thrust coefficient includes the duct thrust. The total thrust is over-predicted by 1 percent and the torque is under-predicted by 6.6 percent.

*Table I. Comparison between measured and calculated performance coefficients for the ducted propeller at J=0.526 in percentages.*

| | Measured | Calculated | |
|---|---|---|---|
| | | 1st level | 2nd level |
| $K_{Tunit}$ | 100.0 | 101. | 98.0 |
| $K_Q$ | 100.0 | 93.4 | 93.6 |

Next, computations were made for the unsteady flow around the ducted propeller with the rudder following a quasi-steady approach.

The presence of the rudder behind the propeller reduces the inflow at the propeller plane and therefore induces a *physical* blockage which can be expressed also as an increment in propeller thrust coefficient. In addition the quasi-steady (and the mixing-plane) method causes a non-physical change of the inflow at the propeller plane, which will be manifested also in the form of a thrust coefficient increase in the case when the propeller block is rotating in front of a non-rotating one with solid surfaces. Henceforth this interaction between blocks will be referred to as *numerical* or *computational* blockage.

Three locations of the interface between the rotating propeller block and non-rotating rudder block were analyzed. The aim was to investigate the numerical blockage. The first location was very close to the rudder, at an axial distance corresponding approximately to the location of the duct trailing edge.

The second one was at the downstream edge of the hub. The third one was somewhere between the blade trailing edge and the downstream edge of the hub.

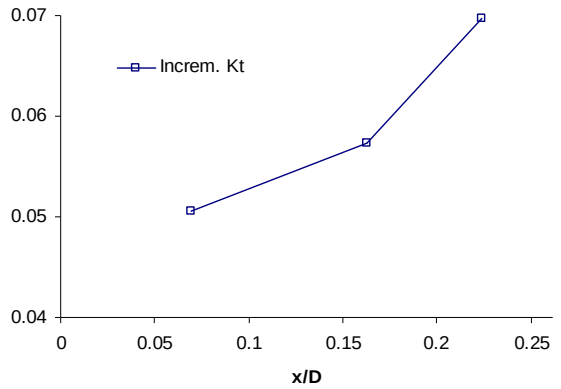


*Figure 6a. Influence of the interface location on propeller thrust. Propeller TE at x/D=0; rudder LE at x/D=0.262.*

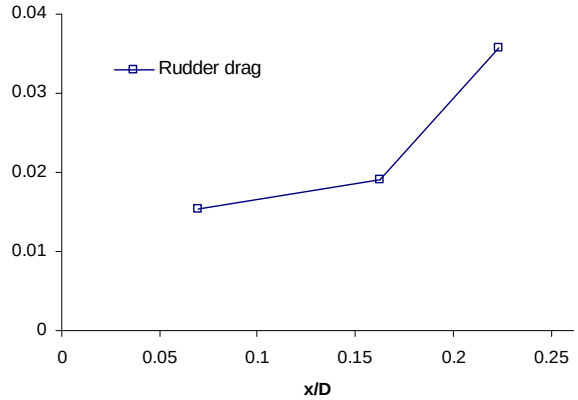


*Figure 6b. Influence of the interface location on rudder drag. Propeller TE at x/D=0; rudder LE at x/D=0.262.*

Figure 6a shows the influence of the location of the interface between the rotating and non-rotating blocks on propeller thrust increase. The propeller trailing edge at the root is located at *x/D=0* and the rudder at *x/D=0.262*. As the interface moves farther from the rudder (low *x*/D) the increment of thrust tends to a constant value, which would ideally correspond to a value free of computational blockage. Figure 6b shows the variation of the rudder drag with the interface distance and the same tendency is observed.

Similar trends were obtained for test computations made using the mixing-plane approach. The latter test calculations were made using a medium size grid (2nd level).

Table II summarizes the results obtained from computations made with the interface located at approximately *x/D*=0.07. In principle the effect of the duct is to increase the *physical* flow blockage on the propeller as compared to the *physical* blockage resulting from an open propeller. In a ducted propeller the contraction of the flow is usually delayed to the duct trailing edge. An *effective* distance between propeller and rudder could be defined for ducted propellers taking as reference distance to the rudder the duct trailing edge instead of the propeller plane. For this particular case such distance is very small, which partially explain the large blockage effect. Additionally some numerical blockage may still be present.

*Table II. Calculated thrust and torque coefficients for the old ducted propeller at J=0.526 (fine grid).*

| | Without rudder | With rudder |
|---|---|---|
| $K_T$ blades | 0.145 | 0.200 |
| $K_T$ blades+duct | 0.183 | 0.235 |
| $K_T$ blades+hub+duct+rudder | | 0.217 |
| $K_Q$ | 0.0279 | 0.0356 |

## FLOW ANALYSIS

Figures 7 and 8 show the pressure contours for the ducted propeller without and with rudder respectively. Low pressure areas are displayed at the propeller leading edge and tip regions including the duct inner surface, which suggests that the propeller is over-pitched for the new design condition. The excess of pitch is noticeable at the outer radial stations. Low pressure areas are also found on the rudder leading edge caused by the propeller induced circumferential flow. Such areas are visible on the lower-right and upper-left side of the rudder in Figures 8 and 9, and are not so much extended and intense as those on the blade suction side.

Figures 10 and 11 show the pressure contours from a back view. Low pressure areas on the pressure side of the blades are displayed at the propeller trailing edge near the tip, which suggests that in the original blade the trailing edge is somewhat bent in order to reduce the pitch. Figure 12 shows a detail view of the blade pressure side. A low pressure peak is seen at the trailing edge.

Figures 13 and 14 show respectively a top and bottom view of the ducted propeller unit with the rudder. The limiting streamlines are shown on the solid surfaces. Flow detachment is illustrated on the outer

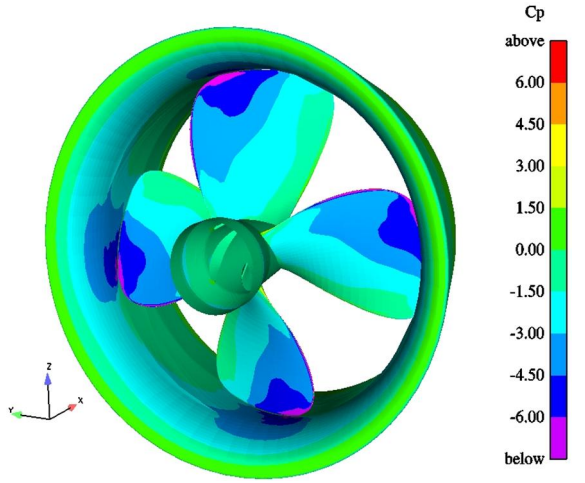


*Figure 7. Pressure distribution on the ducted propeller without rudder. J=0.526*

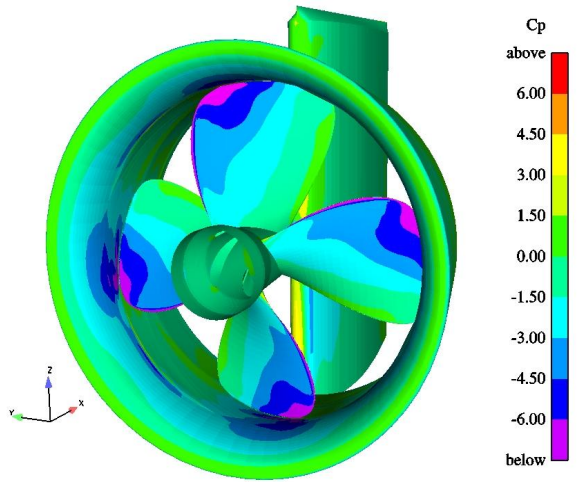


*Figure 8. Pressure distribution on the ducted propeller and rudder surfaces. J=0.526*

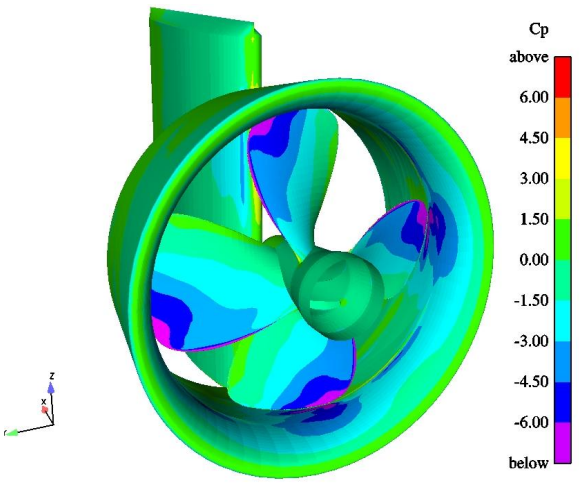


*Figure 9. Pressure distribution on the ducted propeller and rudder surfaces. Starboard side. J=0.526*

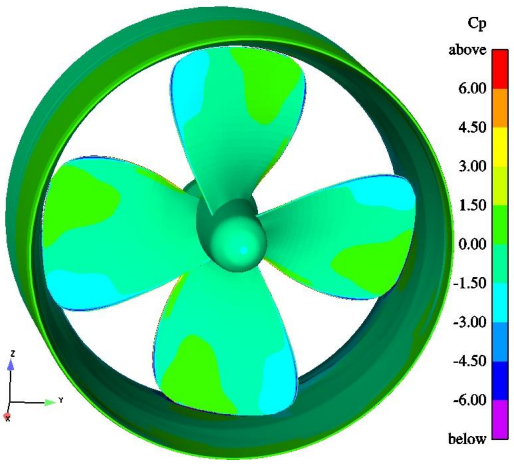


*Figure 10. Pressure distribution on the ducted propeller without rudder. Back view. J=0.526*

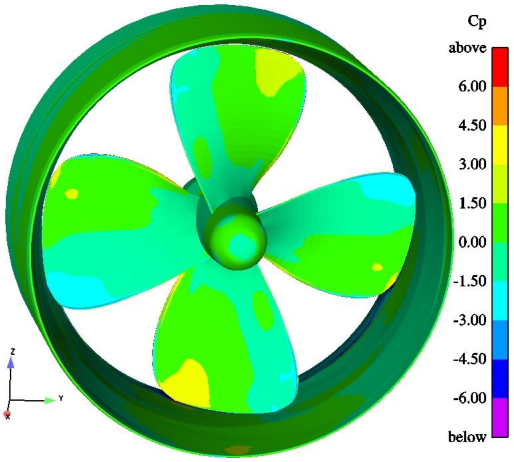


*Figure 11. Pressure distribution on the ducted propeller and rudder surfaces. Back view. J=0.526 (The rudder is not shown to facilitate the illustration)*

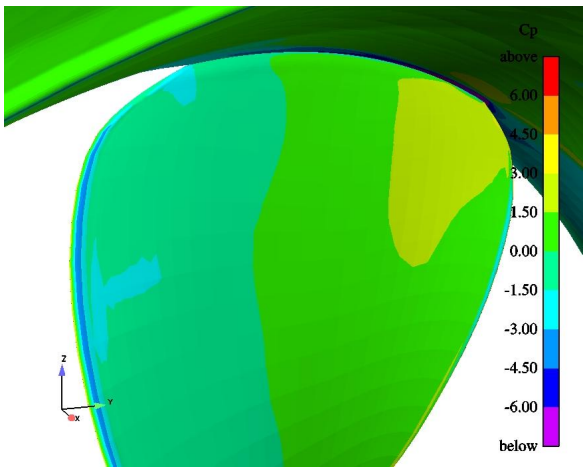


*Figure 12. Detail of pressure distribution on the propeller trailing edge on the pressure side of the blade. J=0.526*

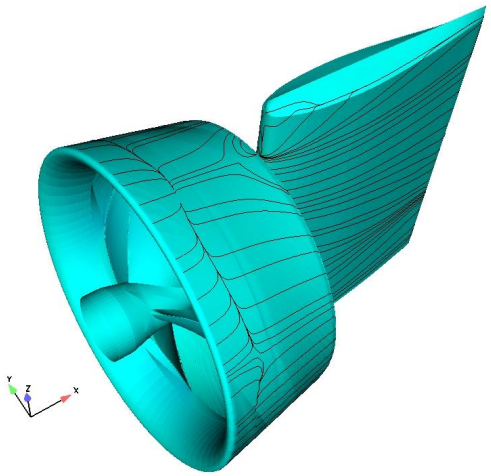

*Figure 13. Limiting streamlines on the duct and rudder surfaces. Top view. J=0.526*

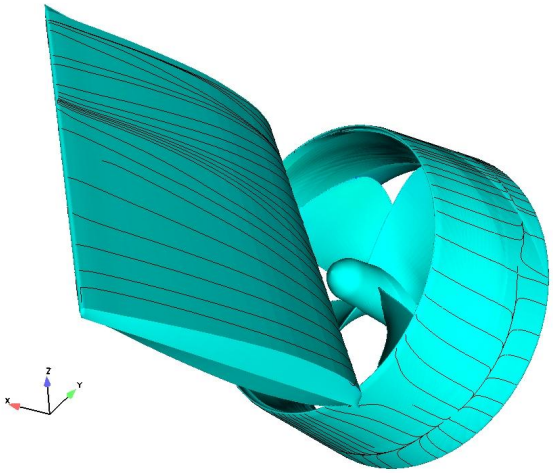

*Figure 14. Limiting streamlines on the duct and rudder surfaces. Bottom view. J=0.526*

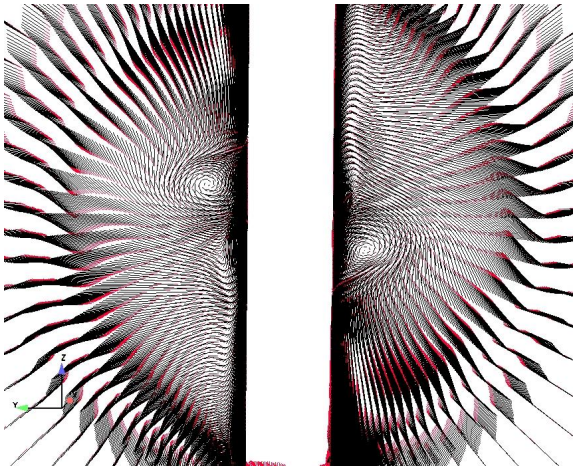

*Figure 15. Arrows indicating the flow direction on a plane perpendicular to the rudder symmetry plane at an axial location near the mid-chord of the rudder profile. Front view. Arrow tips in red. J=0.526*

surface of the duct both at the leading edge area and at the trailing edge in front of the rudder. This situation is expected to be less severe at full scale.

Two vortical structures can be identified on the rudder surfaces in Figures 13 and 14 as a concentration of streamlines near the trailing edge. They are visualized in Figure 15 where arrow vectors show the flow direction on a plane perpendicular to the rudder symmetry plane at an axial location near the mid-chord of the rudder profile. They result from the impinging of the rotating flow on the rudder surfaces. The delayed contraction of the flow is apparent from the direction of the flow at the periphery of the picture.

## ALTERNATIVE DESIGN

A set of alternative ducted propeller designs were prepared. This section describes one of them.

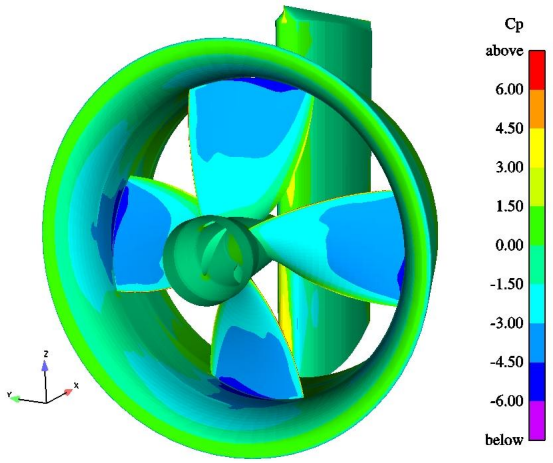


*Figure 16. Pressure distribution on the ducted propeller and rudder surfaces. Alternative design. Port side. J=0.526.*

Full scale measurements provided input data for the calculations made to estimate the pitch reduction required to meet the new engine conditions. A radial chord and skew distribution of Kaplan type was chosen for the blade. The rake for the new design was that of the existing propeller. In this way the relative location of the propeller inside the duct remains unchanged. The design shown in this section was made using NACA a=0.8 camber line with NACA 16 thickness form. The maximum thickness at each section was that of the existing propeller. A vortex lattice lifting surface approach was used for the final adjustment of the new propeller geometry particulars.

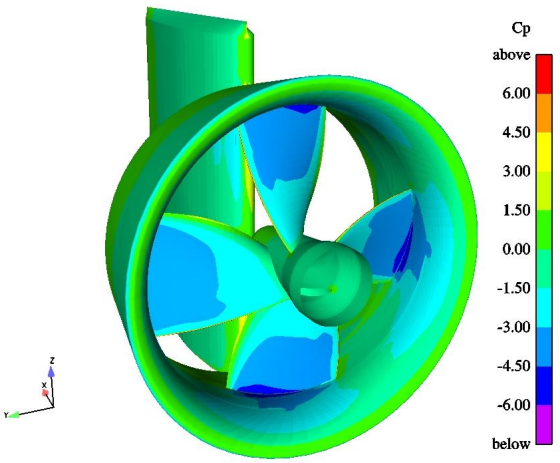


*Figure 17. Pressure distribution on the ducted propeller and rudder surfaces. Alternative design. Starboard side. J=0.526.*

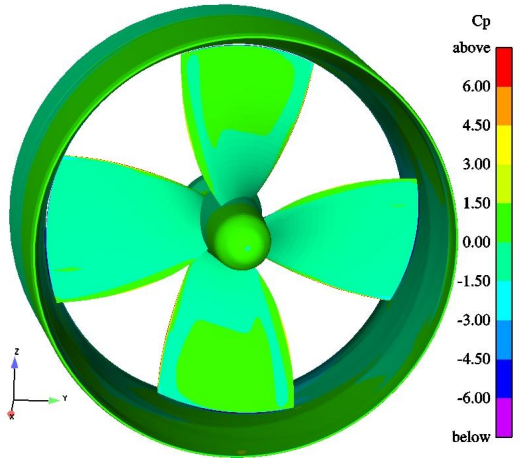


*Figure 18. Pressure distribution on the ducted propeller. Alternative design. Back view. J=0.526. (The rudder is not shown to facilitate the illustration.)*

Figures 16 and 17 show the pressure contours from a port and starboard view, respectively for the new design propeller. The low pressure areas at the leading edge of the old propeller are shifted towards the mid-chord in the new design and the low pressure peak is reduced. Low pressure areas on the rudder leading edge caused by the propeller induced circumferential flow are smaller for the new design due to the reduced propeller loading. Such areas are visible on the upper-left and lower-right side of the rudder.

Figure 18 shows the pressure contours from a back view for the new design propellers. Irregularities on the pressure distribution such as a low pressure peak at the trailing edge and tip in the existing old propeller have been now corrected. Figure 19 shows the blade pressure side in a detail view. A smoother pressure distribution is apparent in the new design.

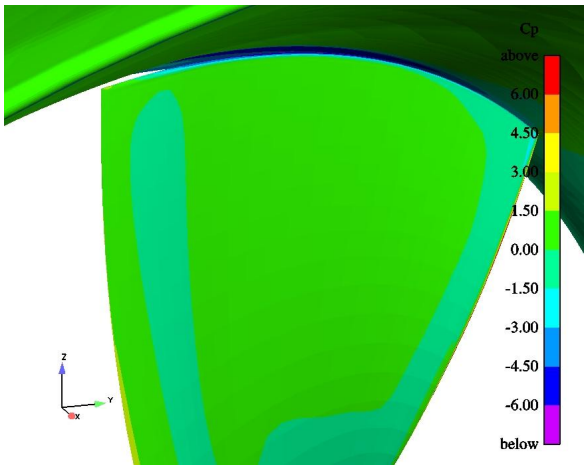


*Figure 19. Detail of pressure distribution on the propeller trailing edge on the pressure side of the blade. Alternative design. J=0.526.*

Figure 20 is indicative of the behavior from the cavitation standpoint of the existing propeller without and with rudder and of the new design. Areas below the vapor pressure are shown in white. The rudder increases somewhat the cavitation at the blade tip due to the decrease of the effective advance number at the propeller plane. Contrary to the existing propeller, the new design is displayed almost free of cavitation at the design condition.

## DISCUSSION OF RESULTS

The flow around a ducted propeller with rudder is basically unsteady. Some simplifications can be made to reduce the computational times in a flow simulation, namely using either a quasi-steady (multiple reference frame) or a mixing-plane approach. In principle a quasi-steady RANS calculations differ in many respects from quasi-steady calculations based on panel methods. In quasi-steady RANS methods an additional provision should be made, not present in panel methods, for minimizing possible *numerical* blockage effects induced by the interface between rotating and non- rotating blocks. This effect will be stronger when the interface is located too close to solid boundaries. Solid boundaries in downstream blocks seem to be more sensitive to blockage than those in upstream

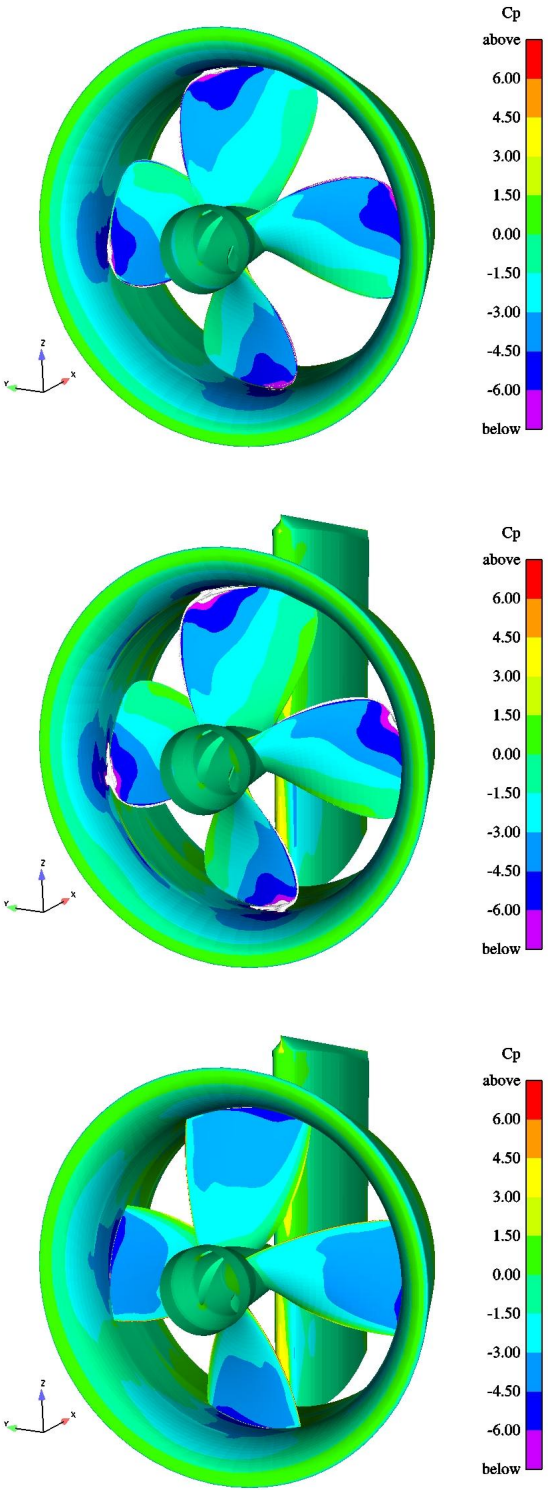


*Figure 20. Comparison of low pressure areas for the existing propeller without rudder (above), with rudder (middle) and new design with rudder (below). J=0.526.*

blocks. Such numerical blockage is also present in the mixing-plane approach.

Additionally the quasi-steady approach presents non-physical features. E.g. any flow disturbance from an upstream non-rotating block seems to rotate when traveling through the downstream rotating one. This means that if a propeller is calculated in the presence of a non-homogeneous inflow by a quasi-steady approach, the axial location of the interface between the rotating and non-rotating part will determine the angular position at which the non-homogeneity will meet the propeller blade. An additional remark is that the simplified numerical approaches cannot be used in oblique flow. Therefore they should be used carefully, being aware of their application limits.

Speaking now about *physical* blockage, the effect of the duct in principle is to increase the flow blockage on the propeller as compared to the blockage resulting from an open propeller. In a ducted propeller working at moderate advance numbers the contraction of the flow is delayed to the duct trailing edge. Usually the physical blockage produced by a rudder is expressed as a function of the distance of the rudder leading edge to the propeller. For ducted propellers an effective distance between propeller and rudder could be defined taking as reference distance to the rudder the duct trailing edge instead of the propeller plane. For this particular case such distance is very small, which partially explain the large blockage effect present in the calculations. Additionally some numerical blockage may still be present.

The steady state calculations of the ducted propeller without rudder show good correlation of the total thrust coefficient, however the torque coefficient is under-predicted in about 6.5 percent. This trend is similar to that presented in Sánchez-Caja et al (2000) for a ducted propeller at the design advance number, where the correlation of torque was somewhat better.

Two vortical structures typical in propellers with rudders were identified using the quasi-steady method. They result from the impingement of the propeller induced rotating flow on the rudder surfaces and are manifested as a concentration of streamlines near the rudder trailing edge on each side of the rudder surface. They are similar to those observed in measurements using PIV technique. Flow detachment was visible on the outer surface of the duct.

Changes in pressure distributions between the computations made without and with rudder are more visible on the propeller pressure side. However, a blockage effect on cavitation is apparent in the calculations. The low pressure area is larger for the ducted propeller with rudder due to the larger flow angle of attack at the tip region caused by the rudder blockage.

## CONCLUSIONS

The flow around an existing old propeller of a reference fishing boat has been analyzed using RANS code FINFLO. The analysis provided enough insight to identify the major issues to be accounted for in the development of the new propeller design. In particular, low pressure areas of interest from the standpoint of cavitation, areas of flow detachment and vortical structures were identified. An alternative design based on NACA sections was made to correct irregularities in the shape of the old propeller and meet the new design condition. The new design was derived from existing full scale measurement on the old propeller and RANS calculations were used to check the quality of the new geometry.

The calculations revealed the appearance of a physical blockage effect at the propeller plane due to the presence of the rudder. The presence of the duct seems to increase the blockage effect from that existing in a conventional propeller. Additionally a non-physical blockage in quasi-steady and mixing-plane approaches was identified as a function of the proximity of the interface between rotating and non-rotating blocks to solid boundaries. In order to minimize the latter blockage the interface should be located far from solid boundaries. Several locations of the interface between rotating and non-rotating blocks were investigated.

## ACKNOWLEDGEMENTS

This work has been made within the European Union SUPERPROP project. The authors wish to thank the partners in the SUPERPROP consortium. Special thanks are given to PESCANOVA for providing the geometries subject to investigation.

## REFERENCES

Greco, L. and Salvatore F. “Numerical Modeling of Unsteady Hydrodynamic Characteristics of a Propeller Rudder Configuration.” 9th Symposium on Practical Design of Ships and Other Floating Structures (PRADS2004). Luebeck-Travemuende, Germany, 2004.

Han, Kai-Jia. “Numerical Optimization of Hull/Propeller/Rudder Configurations”. Doctoral Thesis. Department of Shipping and Marine Technology, Chalmers University of Technology, Göteborg, Sweden, 2008.

Kinnas, S.A., Lee, H., Gu, H., and Natarajan, S. "Prediction of Sheet Cavitation on a Rudder Subject to Propeller Flow," Journal of Ship Research. March 2007

Lee, H., Kinnas, S.A., Gu, H., and Natarajan, S. "Numerical Modeling of Rudder Sheet Cavitation Including Propeller/Rudder Interaction and the Effects of a Tunnel", Fifth International Symposium on Cavitation (CAV2003), Osaka, Japan, November 1-4, 2003.

Li, D.-Q.. "Study of Propeller-Rudder Interaction Based on a Linear Method". International Shipbuilding Progress, Vol. 42, No. 431, 1995, pp. 235-257.

Moriyama, F. "On the Effect of a Rudder on Propulsive Performance", Journal of the Society of Naval Architects of Japan, Vol. 150, 1981.

Sánchez-Caja, A., Rautaheimo, P., Salminen, E., and Siikonen, T., "Computation of the Incompressible Viscous Flow around a Tractor Thruster Using a Sliding Mesh Technique," 7th International Conference in Numerical Ship Hydrodynamics, Nantes (France), 1999.

Sánchez-Caja, A., Rautaheimo, P. and Siikonen, T., "Simulation of Incompressible Viscous Flow Around a Ducted Propeller Using a RANS Equation Solver," 23rd Symposium on Naval Hydrodynamics, Val de Reuil (France), 2000.

Sanchez-Caja, A., Ory, E., Salminen, E., Pylkkänen, J.V. and Siikonen, T. “Simulation of Incompressible Viscous Flow Around a Tractor Thruster in Model and Full Scale.” The 8th International Conference on Numerical Ship Hydrodynamics September 22-25, Busan (Korea), 2003.

Sánchez-Caja, A. and Pylkkänen J.V. "Prediction of Effective Wake at Model and Full Scale Using a RANS Code with an Actuator Disk Model," 2nd International Conference on Maritime Research and Transportation, Ischia, Italy, 28-30 June, 2007.

Sipilä, T.P. Propeller Flows: “Quasi-Steady, Mixing-plane and Time-Accurate Approaches,” Postgraduate Seminar on Heat and Fluid Flow, Espoo, 2008.

Suzuki, H., Toda, Y. and Suzuki, T. "Computation of Viscous Flow around a Rudder Behind a Propeller: Laminar Flow around a Flat Plate Rudder in Propeller Slipstream". 6th International Conference on Numerical Ship Hydrodynamics, Iowa City, 2-5 August, 1993.

Tamashima, M., Matsui, K., Mori, K., and Yamazaki, R., “The method for the predicting the performance of propeller rudder system with rudder angle and its application to the rudder design”, Transactions of the West-Japan Society of Naval Architects, No. 86, 1993 (in Japanese).